ANALYSIS
https://doi.org/10.1038/s41588-022-01039-6

nature genetics

Check for updates

Common variants contribute to intrinsic human brain functional networks

Bingxin Zhao[1,15], Tengfei Li[2,3,15], Stephen M. Smith[4], Di Xiong[5], Xifeng Wang[5], Yue Yang[5], Tianyou Luo[5], Ziliang Zhu[5], Yue Shan[5], Nana Matoba[6,7], Quan Sun[5], Yuchen Yang[6], Mads E. Hauberg[8,9,10,11], Jaroslav Bendl[8,9,12], John F. Fullard[8,9,12], Panagiotis Roussos[8,9,10,12,13], Weili Lin[3,4], Yun Li[5,6,14], Jason L. Stein[6,7] and Hongtu Zhu[3,5,14] ✉

The human brain forms functional networks of correlated activity, which have been linked with both cognitive and clinical outcomes. However, the genetic variants affecting brain function are largely unknown. Here, we used resting-state functional magnetic resonance images from 47,276 individuals to discover and validate common genetic variants influencing intrinsic brain activity. We identified 45 new genetic regions associated with brain functional signatures ($P < 2.8 \times 10^{-11}$), including associations to the central executive, default mode, and salience networks involved in the triple-network model of psychopathology. A number of brain activity-associated loci colocalized with brain disorders (e.g., the *APOE* ε4 locus with Alzheimer's disease). Variation in brain function was genetically correlated with brain disorders, such as major depressive disorder and schizophrenia. Together, our study provides a step forward in understanding the genetic architecture of brain functional networks and their genetic links to brain-related complex traits and disorders.

The human brain is a complex system in which functional organization and communication between brain networks are necessary for behavior and cognition[1,2]. The human brain remains active in the absence of explicit tasks or stimuli, resulting in an intrinsic functional architecture. Using changes in blood oxygen level-dependent signal, resting-state functional magnetic resonance imaging (rsfMRI) captures spontaneous intrinsic brain activity[3]. Specifically, the spontaneous neural activity and nonneural physiological processes within each functional region are quantified by the amplitude of low-frequency fluctuations (ALFFs) in blood oxygen level-dependent time series[4]. Moreover, the interregional correlations in spontaneous neuronal variability are used to construct a functional connectivity matrix, which measures the magnitude of temporal synchrony between each pair of brain regions[3].

rsfMRI has led to the discovery of multiple resting-state networks (RSNs) present in neurotypical human brains, including the default mode, central executive (i.e., frontoparietal), attention, limbic, salience, somatomotor and visual networks[5–7]. Among these RSNs, the central executive, default mode and salience networks are three core neurocognitive networks that support efficient cognition[8]. Accumulating evidence suggests that the functional organization and dynamic interaction of these three networks underlie a wide range of mental disorders, resulting in the triple-network model of psychopathology[8,9]. Supporting this model, differences in RSNs have been detected in multiple neurological and psychiatric disorders relative to neurotypical controls, such as Alzheimer's disease[10], Parkinson's disease[11] and major depressive disorder (MDD)[12].

Twin and family studies have largely reported a low to moderate degree of genetic contributions to intrinsic brain function[13–16]. For example, the family-based heritability estimates of major RSNs ranged from 20% to 40% in the Human Connectome Project (HCP)[17]. In a previous study using about 8,000 UK Biobank (UKB) individuals[18], estimates of the single-nucleotide polymorphism (SNP)-based heritability of amplitude and functional connectivity traits were higher than 30% for some traits. Although there have been multiple candidate gene studies for intrinsic brain activity (such as for *APOE*[19] and *KIBRA*[20]), currently, only a few genome-wide association studies (GWASs)[18,21] have been successfully performed on rsfMRI[13]. This is likely due to both insufficient sample size for GWAS discovery and weaker genetic effects on brain function than structure[18,22,23]. It is also known that functional connectivity traits in rsfMRI are typically noisier than brain structural traits measured in other neuroimaging modalities. In addition, imaging batch effects[24] (e.g., image acquisition, processing procedures and software) may cause additional technical variability in rsfMRI analyses[25], making GWAS meta-analysis and independent replication particularly challenging. Therefore, genetic variants influencing intrinsic brain activity have remained largely undiscovered, and their shared genetic influences with other complex traits and clinical outcomes are unknown.

[1]Department of Statistics, Purdue University, West Lafayette, IN, USA. [2]Department of Radiology, University of North Carolina at Chapel Hill, Chapel Hill, NC, USA. [3]Biomedical Research Imaging Center, School of Medicine, University of North Carolina at Chapel Hill, Chapel Hill, NC, USA. [4]Wellcome Centre for Integrative Neuroimaging, FMRIB, Nuffield Department of Clinical Neurosciences, University of Oxford, Oxford, UK. [5]Department of Biostatistics, University of North Carolina at Chapel Hill, Chapel Hill, NC, USA. [6]Department of Genetics, University of North Carolina at Chapel Hill, Chapel Hill, NC, USA. [7]UNC Neuroscience Center, University of North Carolina at Chapel Hill, Chapel Hill, NC, USA. [8]Department of Psychiatry, Icahn School of Medicine at Mount Sinai, New York, NY, USA. [9]Friedman Brain Institute, Icahn School of Medicine at Mount Sinai, New York, NY, USA. [10]iPSYCH, The Lundbeck Foundation Initiative for Integrative Psychiatric Research, Aarhus, Denmark. [11]Centre for Integrative Sequencing (iSEQ), Aarhus University, Aarhus, Denmark. [12]Department of Genetics and Genomic Science and Institute for Multiscale Biology, Icahn School of Medicine at Mount Sinai, New York, NY, USA. [13]Mental Illness Research, Education, and Clinical Center (VISN 2 South), James J. Peters VA Medical Center, Bronx, NY, USA. [14]Department of Computer Science, University of North Carolina at Chapel Hill, Chapel Hill, NC, USA. [15]These authors contributed equally: Bingxin Zhao, Tengfei Li. ✉e-mail: htzhu@email.unc.edu

To address these challenges, here, we collected individual-level rsfMRI data from four independent studies, including the UKB[26], Adolescent Brain Cognitive Development (ABCD[27]), Philadelphia Neurodevelopmental Cohort (PNC[28]) and HCP[29]. We harmonized rsfMRI processing procedures by following the unified UKB brain imaging pipeline[4,30]. Functional brain regions and corresponding functional connectivity were characterized via spatial independent-component analysis (ICA)[31,32] for 47,276 individuals from multiple ancestries, including 40,425 from UKB. As in previous studies[4,18,21], two parcellations with different dimensionalities[6,33] (25 and 100 regions, respectively) were separately applied in spatial ICA, and we focused on the 76 (21 and 55, respectively) regions that had been previously confirmed to be nonartifactual[4]. Two groups of neuroimaging phenotypes were then generated; the first group contains 76 (node) amplitude traits reflecting the regional spontaneous neuronal activity, and the second group includes 1,695 (i.e., $21\times20/2+55\times54/2$) (edge) functional connectivity traits that quantify the interregional coactivity, as well as six global functional connectivity measures[18] (Methods and Supplementary Fig. 1). These 1,777 traits were then used to explore the genetic architecture of intrinsic brain activity. Our GWAS results can be easily explored and downloaded through the Brain Imaging Genetics Knowledge Portal at https://bigkp.org.

Results

Genetics of the intrinsic brain functional architecture. SNP heritability was estimated for the 1,777 intrinsic brain activity traits via GCTA[34] using UKB individuals of British ancestry ($n=34,691$). The mean heritability (h^2) estimate was 27.5% (range = (10.6%, 38.6%), standard error = 6.1%) for the 76 amplitude traits, all of which remained significant after adjusting for multiple comparisons by using the Benjamini–Hochberg procedure to control false discovery rate (FDR) at the 0.05 level (1,777 tests; Fig. 1a and Supplementary Table 1). Among the 1,701 functional connectivity traits, 1,192 had significant (again at 5% FDR) heritability, with estimates varying from 3% to 60% (mean = 9.3%, standard error = 5.6%). Ten functional connectivity traits had heritability higher than 30%, including four global functional connectivity measures (Supplementary Fig. 1) and six pairwise functional connectivity traits (Fig. 1b). These most heritable traits were most related to the central executive, default mode and salience networks in the triple-network model of psychopathology[8]. To examine whether intrinsic brain activity within the triple network had higher heritability, we classified the 76 amplitude traits into two categories: (1) fully or partially within the triple network and (2) outside the triple network. Correspondingly, the 1,695 pairwise functional connectivity traits were classified as follows: (1) within the triple network, (2) outside the triple network and (3) between the triple and non-triple networks. We found that amplitude traits within the triple network had significantly higher heritability than those outside the triple network (mean = 30.9% versus 22.6%, $P=8.5\times10^{-11}$, two-sided Wilcoxon rank test) (Fig. 1c). Similarly, functional connectivity traits within the triple network had higher heritability than interactions outside the triple network or between the triple and non-triple networks (mean = 11.9% vs. 6.9%, $P=8.4\times10^{-20}$). Similar results were observed when we limited the comparison between the triple network and two major sensory networks (the visual and motor networks; Supplementary Fig. 2). These results indicate that the three core neurocognitive networks can be robustly detected by spatial ICA and might have a higher level of genetic control. The range of heritability estimates was consistent with previous results[18], suggesting that common genetic variants had a low to moderate degree of contributions to interindividual variability of intrinsic brain activity. The overall genetic effects on both amplitude and functional connectivity were lower than those on brain structure. For example, the average heritability was reported to be 47.6% for diffusion tensor imaging (DTI) traits of brain structural connectivity in white matter tracts[35] and 40% for regional brain volumes measuring brain morphometry[23]. Nevertheless, as shown below, intrinsic brain activity may be more functionally relevant, with stronger genetic connections to brain disorders such as Alzheimer's disease than brain structure.

A GWAS was carried out for 1,777 intrinsic brain activity traits and 9,026,427 common variants in the UKB British sample ($n=34,691$). The Manhattan and quantile-quantile plots can be found in the Brain Imaging Genetics Knowledge Portal server (https://bigkp.org). At the significance level 2.8×10^{-11} ($5\times10^{-8}/1,777$, that is, the standard GWAS threshold, Bonferroni-adjusted for the 1,777 traits), FUMA[36] identified 241 lead independent variants (linkage disequilibrium (LD) $r^2<0.1$), and then characterized 603 significant locus–trait associations with 191 traits (75 amplitude, 111 pairwise functional connectivity and 5 global functional connectivity) in 45 genomic regions (Supplementary Tables 2 and 3 and Supplementary Fig. 3). Global and pairwise functional connectivity traits that had at least 5 significant variants were again most related to the central executive, default mode and salience networks (Supplementary Fig. 4). Of the 14 associated variants that had been identified in the previous GWASs[18], 12 were in LD ($r^2\geq0.6$) with our significant variants, most of which were associated with amplitude traits. In summary, our analyses identify many new variants associated with intrinsic functional signatures and illustrate the global genetic influences on functional connectivity across the whole brain.

Replication and the effect of ancestry. We aimed to replicate our results in UKB British GWASs using other independent datasets. We first examined the reproducibility and stability of the intrinsic brain activity traits (Supplementary Note). Overall, moderate-to-good stability of the UKB-trained ICA regions was observed across different ancestry groups in independent datasets, suggesting that we used a set of well-defined and biologically meaningful traits in GWASs (Supplementary Figs. 5 and 6 and Supplementary Table 4). We then repeated GWASs on a combined dataset of individuals of white ancestry in the newly released UKB phase 4 data and individuals of white but non-British ancestry in the UKB phases 1 to 3 data (UKBW, total $n=5,056$). We checked whether the 603 significant locus–trait associations detected in UKB British GWASs could be replicated. We found that 118 associations (19.6%) passed the 8.2×10^{-5} (i.e., 0.05/603) Bonferroni significance level in the UKBW GWAS, and 440 (73.0%) were significant at the nominal 0.05 level. All the 440 associations had concordant directions in the two independent GWASs, showing a high degree of generalizability of our GWAS findings among European-ancestry cohorts (Supplementary Fig. 7).

Next, we performed GWASs on three non-UKB European-ancestry cohorts, including the ABCD European (ABCDE; $n=3,821$), HCP European ($n=495$) and PNC ($n=510$). After meta-analyzing the four European-ancestry GWASs (total $n=9,882$), the number of associations passing the Bonferroni significance level increased to 131 (21.7%), which were involved in 17 of the 45 identified genomic regions. We also performed GWASs on four non-European validation datasets: the UKB Asian (UKBA; $n=446$), UKB Black (UKBBL; $n=232$), ABCD Hispanic (ABCDH; $n=768$) and ABCD African American (ABCDA; $n=1,257$). We meta-analyzed these four non-European GWAS (total $n=2,703$) and found that one association passed the Bonferroni significance level and 34 (5.6%) were significant at the nominal 0.05 level and had the same direction as in discovery GWASs. Moreover, we performed a third meta-analysis to combine all the eight validation datasets, after which the number of replicated associations was 122 (20.2%) at the Bonferroni significance level, and the number of replicated genomic regions increased to 18. These results are summarized in Supplementary Table 5. Overall, our results suggest that a large proportion (18/45, 40%) of associated genomic regions discovered in UKB British GWASs can be replicated in independent studies at the Bonferroni significance

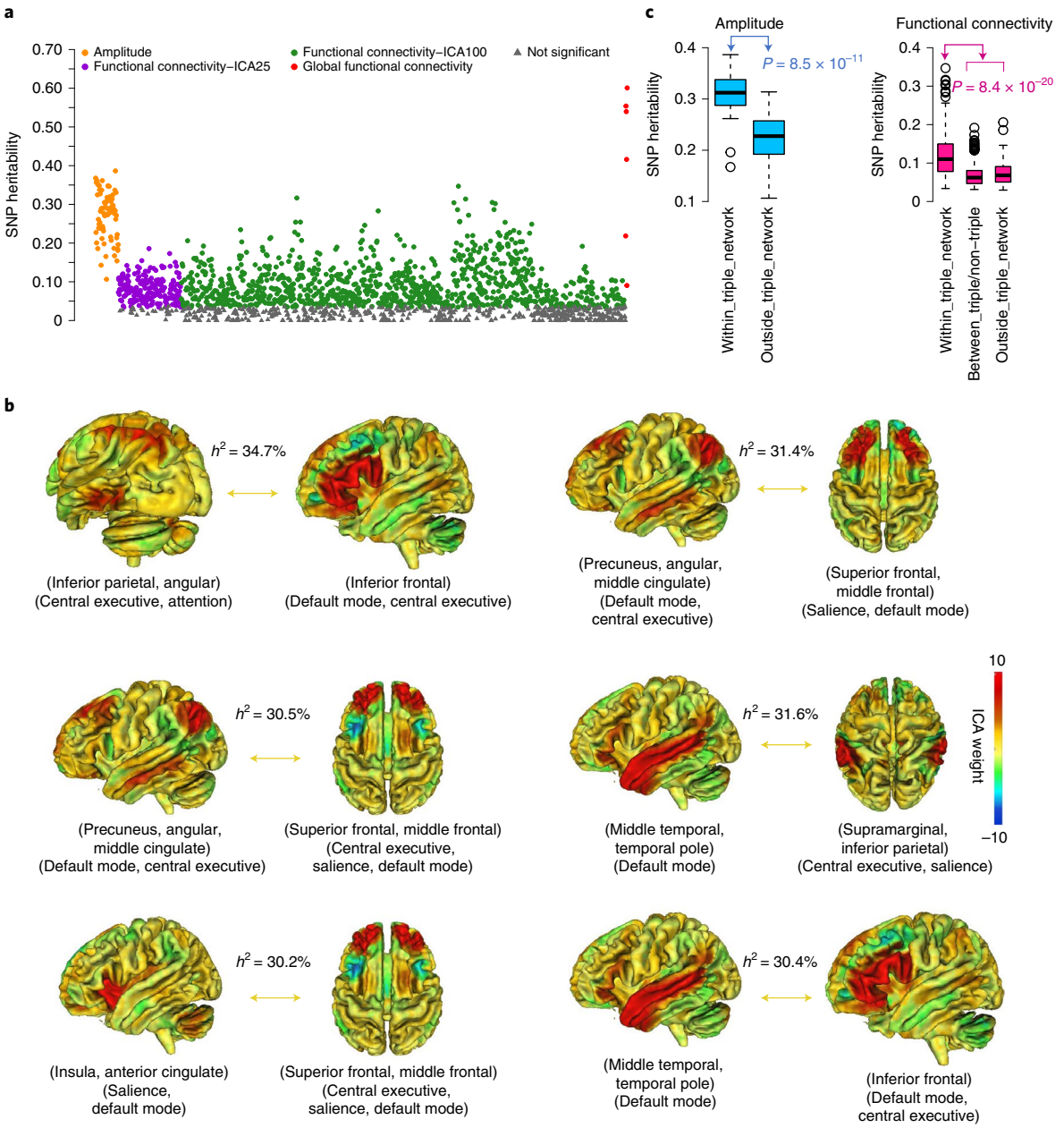

Fig. 1 | SNP heritability analysis of rsfMRI traits. a, Heritability estimates of 1,777 rsfMRI traits of brain activity, including 76 amplitude traits, 1,695 pairwise functional connectivity traits (from two parcellations with 25 and 100 dimensionalities, respectively) and 6 global functional connectivity measures ($n = 34{,}691$ subjects). **b**, Location and functional network of the pairs of functional regions (i.e., nodes) characterized by spatial ICA whose interregional functional connectivity had heritability (h^2) higher than 30%. The color represents the weight profile of the ICA node. For example, the functional connectivity between two ICA nodes mainly over the inferior parietal, angular and inferior frontal regions had $h^2 = 34.7\%$. **c**, Comparison of the heritability within the triple network (i.e., the three core neurocognitive networks: central executive, default mode and salience) and the heritability outside the triple network. *P* value of the two-sided Wilcoxon rank test was used to evaluate the difference ($n = 76$ heritability estimates for amplitude traits and 1,695 heritability estimates for functional connectivity traits). The box of the displayed boxplots starts in the first quartile (25%, denoted as Q_1) and ends in the third (75%, Q_3). The line inside the box represents the median. There is a segment to the furthest observations (the minima and maxima) on each side of the box, without counting the boxplot outliers (if any). The boxplot outliers (represented with circles, if any) are observations that are larger than $Q_3 + 1.5 \times (Q_3 - Q_1)$ or smaller than $Q_1 - 1.5 \times (Q_3 - Q_1)$.

level, despite the fact that these studies may use different imaging protocols or MRI scanners and recruit participants from different age groups. In addition, we used polygenic risk scores[37] (PRSs) derived from UKB British GWASs for further evidence of replication (Supplementary Note). Our PRS results illustrate the overall consistency of genetic effects in European-ancestry cohorts and show that there may be population-specific influences on brain function in non-European-ancestry cohorts, although much smaller sample sizes and difficulty in conducting cross-ancestry PRS strongly limit the interpretability of these analyses (Supplementary Table 6).

The shared genetic loci with brain-related complex traits and disorders. To evaluate the shared genetic components between intrinsic brain activity and other complex traits, we carried out

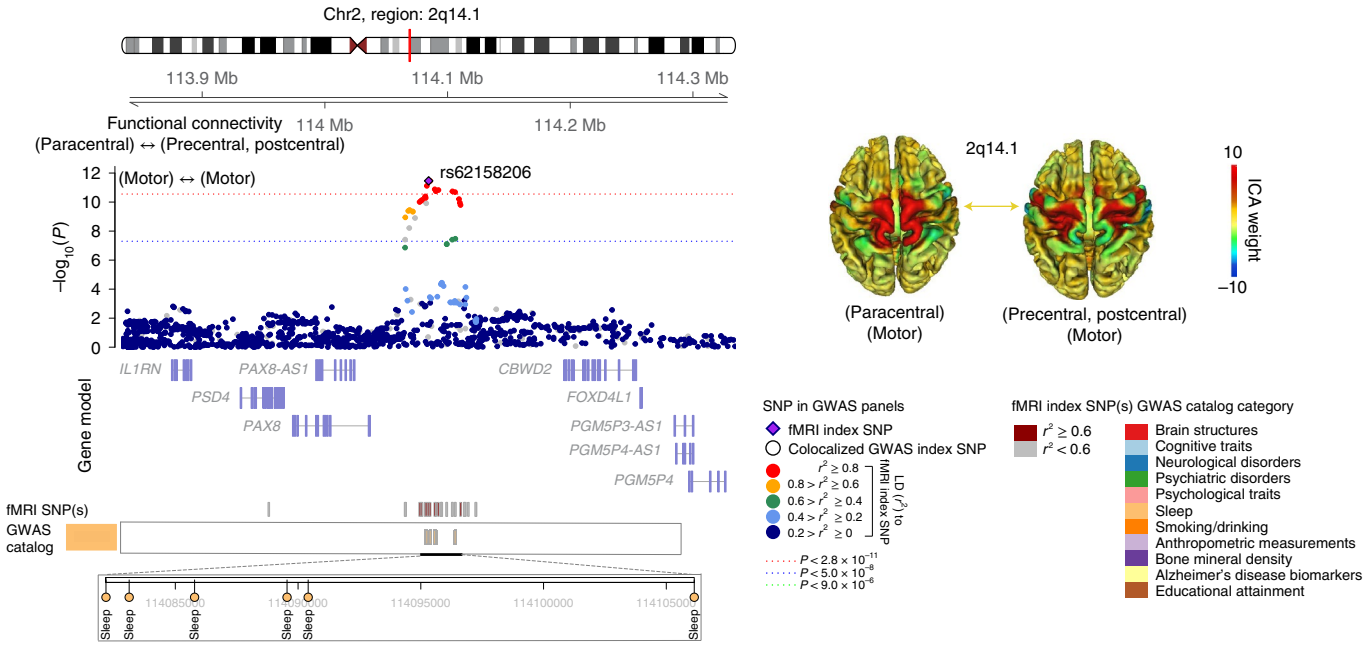

Fig. 2 | Selected genetic locus associated with both rsfMRI trait of brain activity and brain-related complex traits. At 2q14.1, we observed colocalization (LD $r^2 \geq 0.6$) between the functional connectivity of the motor network and sleep traits (shared index SNP rs62158206). The location of the displayed rsfMRI trait (functional connectivity between paracentral and precentral and postcentral regions) is illustrated (right).

association lookups for independent significant variants (and their LD tags (i.e., variants with LD, $r^2 \geq 0.6$)) detected in UKB British GWASs. In the NHGRI-EBI GWAS catalog[38], our results tagged many variants reported for a wide range of complex traits in different trait domains, such as neurological and psychiatric disorders, cognitive performance, education, sleep, smoking/drinking, brain structure and anthropometric traits. Below, we highlight colocalizations in a few selected genomic regions.

The index variants rs429358 (*APOE*), rs71352238 (*TOMM40*), rs184017 (*TOMM40*) and rs157592 (*APOC1*) in the 19q13.32 region had genetic effects on the amplitude of many functional brain regions that were strongest in the default mode, central executive (i.e., frontoparietal), attention and visual networks (Extended Data Fig. 1 and Supplementary Fig. 8). It is well known that 19q13.32 is a risk locus of Alzheimer's disease, and rs429358 is one of the two variants in the *APOE* ε4 locus. In this region, we tagged variants associated with dementia and decline in mental ability, including Alzheimer's disease[39–41], frontotemporal dementia[42], cerebral amyloid angiopathy[43], cognitive decline[44] and cognitive impairment test score[45], as well as many biomarkers of Alzheimer's disease, such as neurofibrillary tangles[43], neuritic plaque[43], cerebral amyloid deposition[46], cerebrospinal fluid protein levels[45] and cortical β-amyloid load[47]. Altered amplitude activity has been widely reported in patients of cognitive impairment and Alzheimer's disease[48]. The brain degeneration related to Alzheimer's disease may begin in the frontoparietal regions[49] and is associated with dysfunction of multiple RSNs, especially the default mode network[10]. Our findings suggest the shared genetic influences between intrinsic neuronal activity and brain atrophy of Alzheimer's disease. Neuroimaging traits from rsfMRI could be used as biomarkers for future medication developments targeting *APOE* ε4.

The 17q21.31 region was associated with functional connectivity over the inferior frontal, middle frontal, superior frontal, middle temporal and supplementary motor area regions in the default mode and salience networks (Supplementary Fig. 9). Variants in LD with rsfMRI index variants in this region have been widely related to neurological disorders (e.g., Parkinson's disease[50–52]) and brain-related related complex traits (Supplementary Note). In addition, the 2p16.1 (Extended Data Fig. 2 and Supplementary Fig. 10) and 5q15 (Supplementary Fig. 11) regions were mainly associated with interactions among the central executive, default mode and salience networks. We observed colocalizations with psychiatric disorders (e.g., schizophrenia[53], MDD[54], depressive symptoms[55] and autism spectrum disorder[56]), psychological traits (e.g., neuroticism[57] and well-being spectrum[58]), sleep[59], cognitive traits (e.g., intelligence[60]) and educational attainment[61]. Dysregulated triple-network interactions were frequently reported in patients of schizophrenia[62], depression[63] and autism spectrum disorder[64]. Similarly, the 2q24.2 (Supplementary Fig. 12) and 10q26.13 (Supplementary Fig. 13) regions had genetic effects on functional connectivity traits involved in the central executive, default mode, salience, attention and limbic networks. In these two regions, our identified variants tagged those that have been implicated with schizophrenia[65], educational attainment[61], cognitive traits (e.g., cognitive ability[66]) and smoking/drinking (e.g., smoking status[67] and alcohol consumption[68]). We also observed colocalizations in some other genomic regions, such as in 2q14.1 region (Fig. 2 and Supplementary Fig. 14) with sleep traits[59], in 3p11.1 (Supplementary Fig. 15) with cognitive traits (e.g., intelligence[69] and math ability[61]) and in 5q14.3 (Supplementary Fig. 16) with smoking[68] and autism spectrum disorder[70]. All of these results are summarized in Supplementary Table 7. In summary, intrinsic brain function has wide genetic links to many brain-related complex traits and clinical outcomes, especially neurological and psychiatric disorders and cognitive traits. Integration of GWASs of brain function with these clinical outcomes may help to explain the underlying brain functional mechanisms leading to risk for these disorders.

Genetic correlations with brain structure, brain disorders and cognition. The intricate brain neuroanatomical structure is fundamental in supporting brain function. To explore whether genetically mediated brain structural changes were associated with brain function, we examined pairwise genetic correlations between 484 heritable intrinsic brain activity traits with $h^2 > 10\%$ and 315 brain structure traits via the LD score regression (LDSC)[71], including

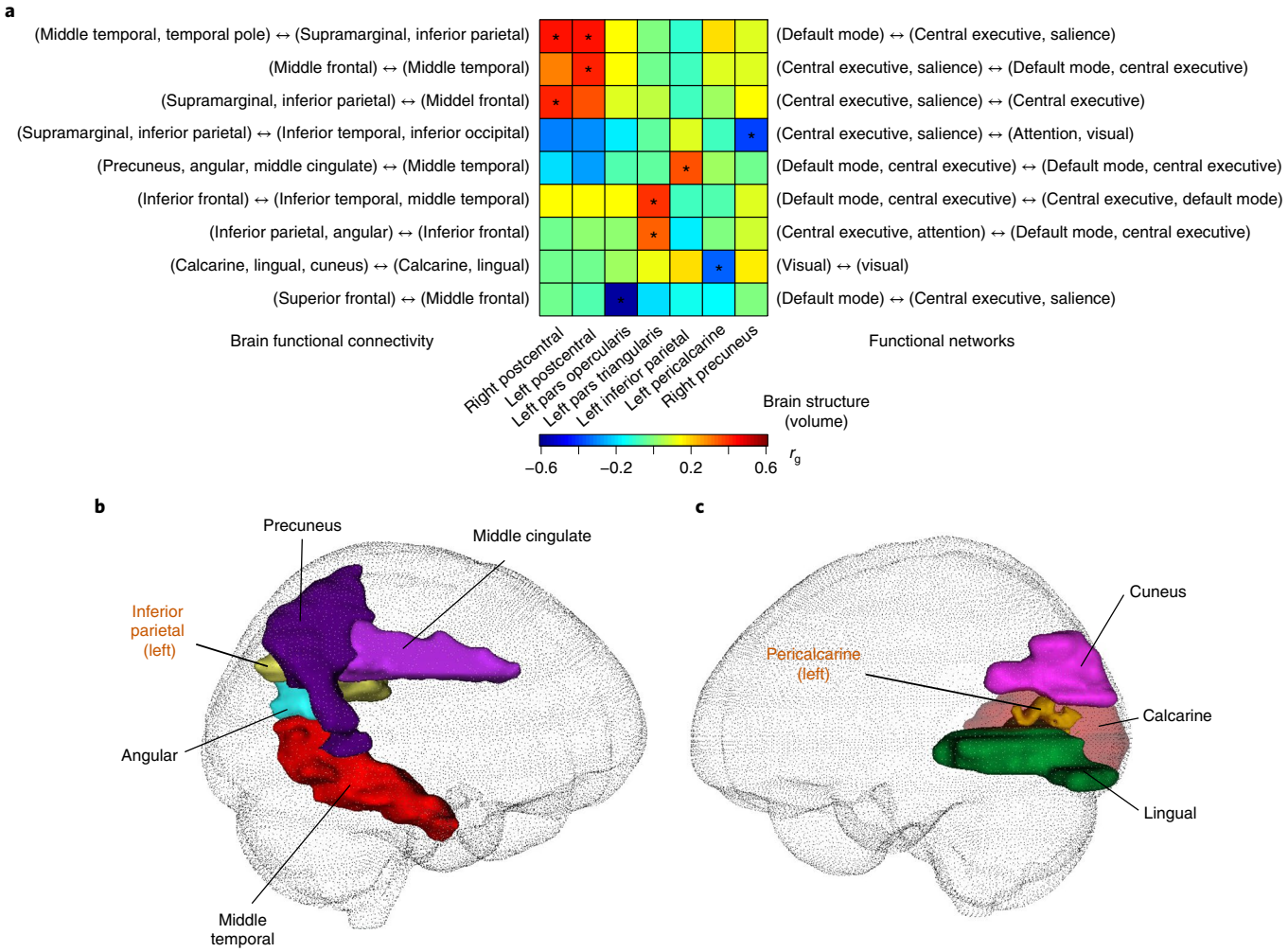

Fig. 3 | Selected pairwise genetic correlations between functional connectivity traits and regional brain volumes. a, The left *y* axis lists the location of functional connectivity traits, the right *y* axis shows the associated functional networks and the *x* axis provides the name of regional brain volumes. The colors represent genetic correlations (r_g). The asterisks highlight significant associations after controlling the FDR at the 0.05 level. **b**, Location of the left inferior parietal (name labelled in orange color) and its neighboring brain regions (names labelled in black color) whose functional connectivity strengths were genetically correlated with the left inferior parietal volume. The colors describe different brain regions. **c**, Location of the left pericalcarine (name labelled in orange color) and its neighboring brain regions (names labelled in black color) whose functional connectivity strengths were genetically correlated with the left pericalcarine volume.

100 regional brain volumes[23] and 215 DTI traits of brain structural connectivity in white matter tracts[35]. There were 63 significant pairs between 46 intrinsic brain functional traits and 31 brain structural traits at the FDR 5% level (315×484 tests, |genetic correlations| range = (0.2, 0.57), P range = $(4.7 \times 10^{-10}, 2 \times 10^{-5})$, Supplementary Table 8).

We found significant genetic correlations between regional brain volumes and functional connectivity strengths (|genetic correlations| range = (0.28, 0.57), P range = $(1.1 \times 10^{-8}, 2 \times 10^{-5})$; Supplementary Fig. 17). Most of the observed correlations were related to higher-order brain functional networks, particularly the default mode, salience and central executive networks. We observed spatial colocalizations between regional brain volumes and their genetically correlated functional connectivity traits. Specifically, all these genetically correlated pairs were overlapped or spatially close to each other (within 30 mm; Supplementary Note). For example, the left inferior parietal lobule volume exhibited genetic correlations with connectivity strengths over multiple pairs of brain regions that were known to be a part of the default mode and central executive networks (genetic correlations = 0.35, $P = 1.2 \times 10^{-5;}$ Fig. 3a,b). The inferior parietal has been implicated to be associated with language function and is connected with the Broca's region via the superior longitudinal fasciculus (SLF)[72–74]. The left pericalcarine volume was genetically correlated with the connectivity strengths among its neighboring regions, including the calcarine, cuneus and lingual in the visual network (Fig. 3c). More spatial overlap/proximity examples can be found in Supplementary Note and Supplementary Fig. 18.

Significant genetic correlations were also observed between brain structural connectivity and functional connectivity (|genetic correlations| range = (0.2, 0.53), P range = $(4.7 \times 10^{-10}, 2 \times 10^{-5})$, Supplementary Fig. 19). The SLF and corpus callosum manifested strong genetic correlations with the interactions of functional networks (Fig. 4a). Specifically, we observed significant genetic correlations between SLF and connectivity strengths over multiple pairs of brain regions, including the frontal, parietal and temporal regions (|genetic correlations| range = (0.32, 0.50), $P < 1.9 \times 10^{-5}$, Fig. 4b). In addition, the corpus callosum was genetically associated with functional connectivity of multiple brain regions, such as the precuneus (|genetic correlations| range = (0.39, 0.53), $P < 1.3 \times 10^{-5}$; Fig. 4c). See Supplementary Note for more details and interpretations

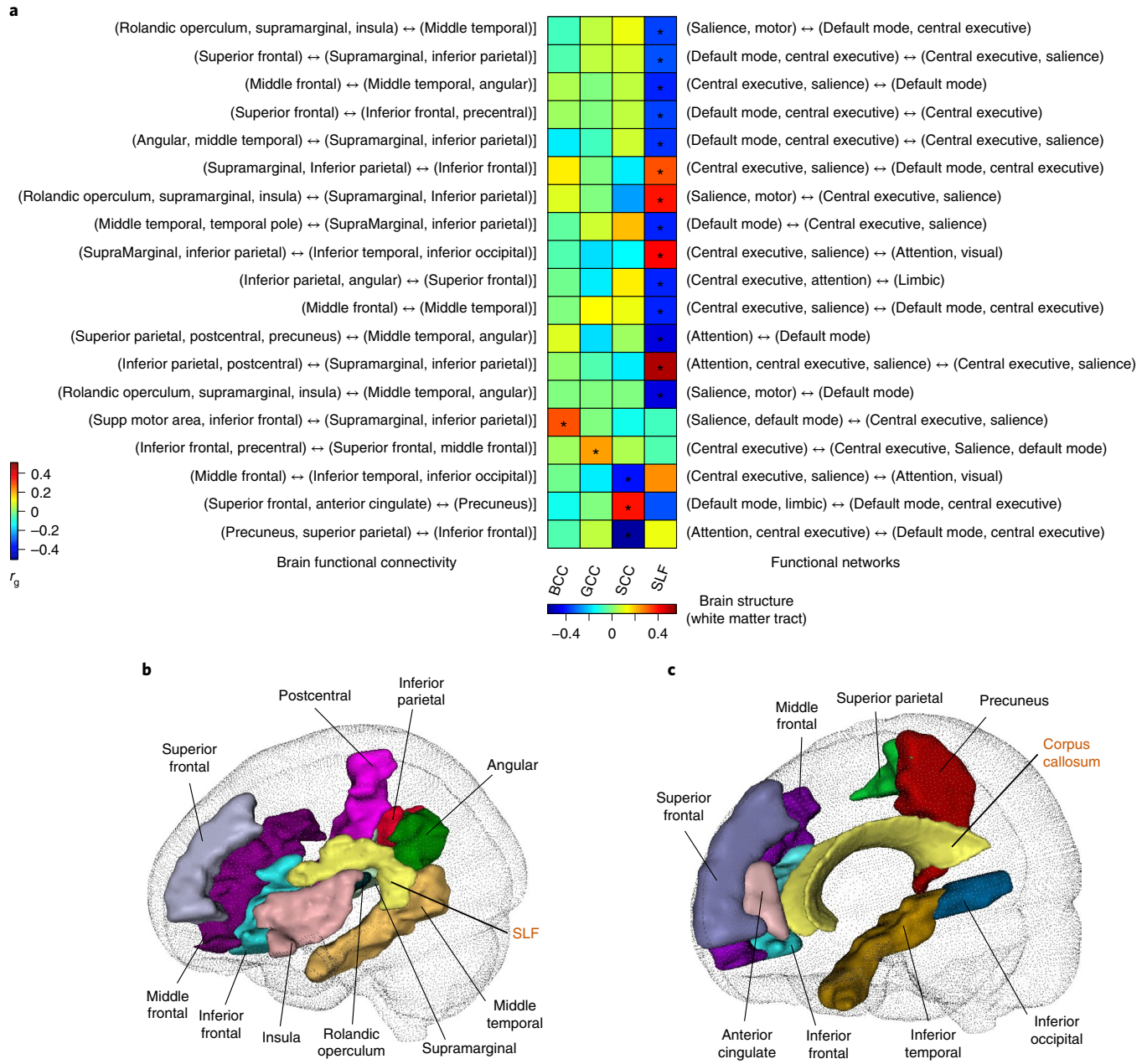

Fig. 4 | Selected pairwise genetic correlations between functional connectivity traits and fractional anisotropy of white matter tracts. a, The asterisks highlight significant associations after controlling the FDR at 0.05 level. The left *y* axis lists the location of functional connectivity traits, the right *y* axis shows the associated functional networks and the *x* axis provides the name of white matter tracts. The colors represent genetic correlations (r_g). BCC, body of corpus callosum; GCC, genu of corpus callosum; SCC, splenium of corpus callosum. **b**, Location of the SLF (left part, name labelled in orange color) and its neighboring brain regions (names labelled in black color) whose functional connectivity strengths were genetically correlated with the fractional anisotropy of SLF. The colors describe different brain regions. **c**, Location of the CC (name labelled in orange color) and its neighboring brain regions (names labelled in black color) whose functional connectivity strengths were genetically correlated with the fractional anisotropy of CC. FA, fractional anisotropy.

of these results. Besides functional connectivity traits, amplitude traits also had significant genetic associations with white matter tracts (Supplementary Fig. 20). Overall, 72.7% of these genetically correlated brain functional and structural traits show high congruity in spatial location and the involved functions (within 30 mm; Supplementary Note). There has been growing interest to understand how brain topography interacts with brain functional networks[75], and our results indicate that genetic changes in brain structure may also impact brain function.

Next, we examined the genetic correlations between the 484 intrinsic brain activity traits and 10 neuropsychiatric disorders and cognitive traits (Supplementary Table 9). We found 79 significant genetic correlations with 42 intrinsic brain activity traits at the FDR 5% level (10×484 tests, P range $= (7.7 \times 10^{-8}, 8 \times 10^{-4})$; Supplementary Table 10). Particularly, functional connectivity strengths were genetically correlated with several brain disorders, including schizophrenia, MDD, cross disorder (five major psychiatric disorders[76]) and bipolar disorder (|genetic correlations|

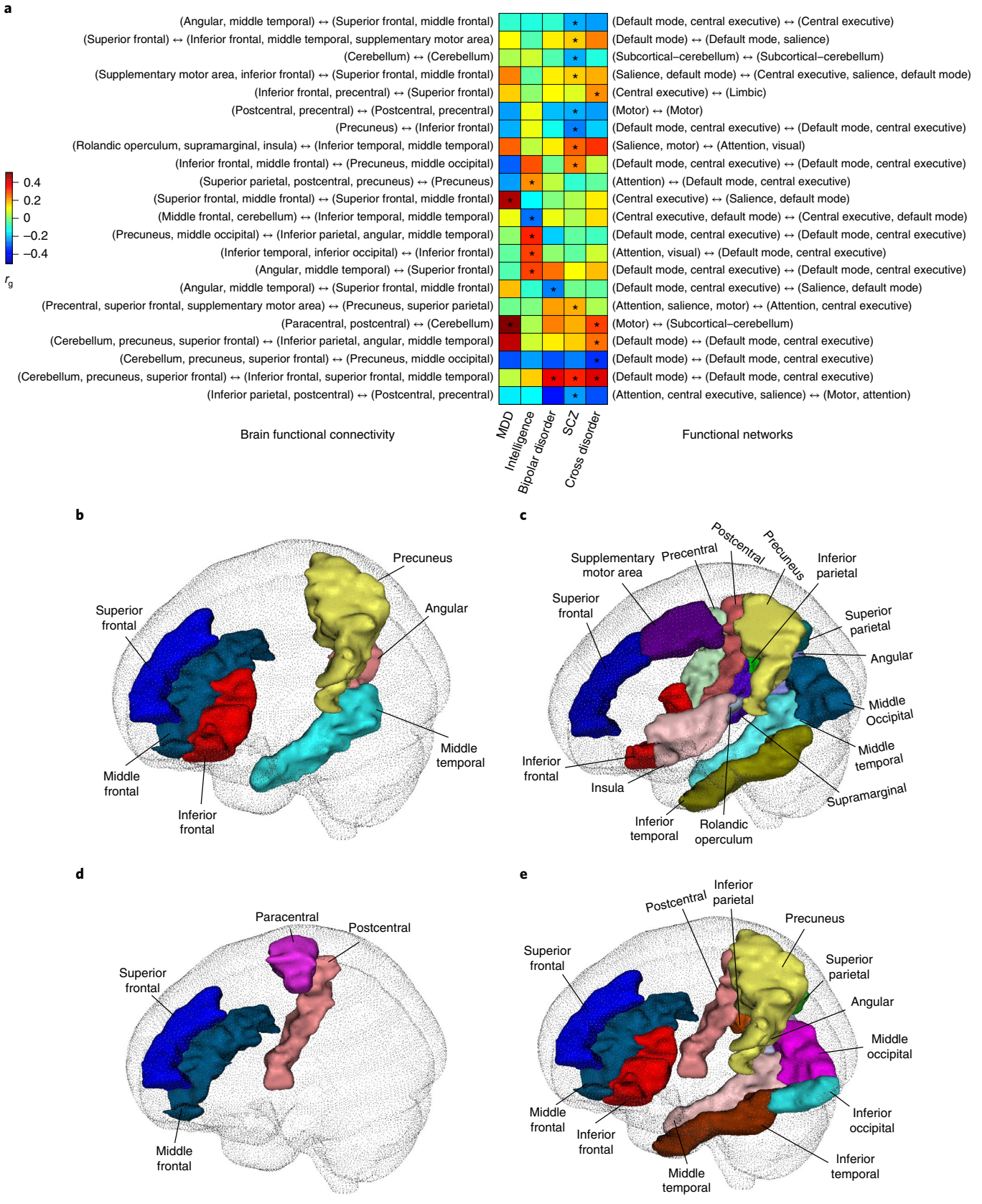

Fig. 5 | Selected pairwise genetic correlations between functional connectivity traits and brain disorders and intelligence. a, The asterisks highlight significant associations after controlling the FDR at the 0.05 level. The left *y* axis lists the location of functional connectivity traits, the right *y* axis shows the associated functional networks and the *x* axis provides the name of other complex traits/disorders. The colors represent genetic correlations (r_g). **b**–**e**, Location of the brain regions whose functional connectivity strengths were genetically correlated with bipolar disorder (**b**), schizophrenia (SCZ) (**c**), MDD (**d**) and intelligence (**e**). The colors describe different brain regions.

range = (0.15, 0.5), $P < 8 \times 10^{-4}$; Fig. 5a). A large proportion (72%) of these correlations were related to the triple networks of psychopathology. For example, we observed significant genetic correlations between bipolar disorder and functional interactions among the frontal, middle temporal, precuneus and angular regions, which were largely in the default mode network (Fig. 5b). Several lines of evidence have pointed the possible default mode alterations in bipolar disorder[77]. Moreover, significant genetic correlations were observed between schizophrenia and connection strengths over the frontal, parietal, temporal and cerebellum regions (Fig. 5c) and between MDD and interactions among the frontal and parietal (paracentral and postcentral) regions (Fig. 5d). Deficits of frontotemporal systems, such as impairment in executive functions and learning, are core features of schizophrenia[78]. Previous studies have consistently reported abnormal activation of the frontal and parietal cortices and frontotemporal dysconnectivity in schizophrenia[79]. In addition, genetic correlations were observed between functional connectivity and cognitive traits studied in previous GWASs, including intelligence, cognitive performance, general cognitive function, numerical reasoning and education (Supplementary Fig. 21). Most (98.1%) of these functional connectivity traits were related to the triple networks. For example, intelligence had genetic correlations with connection strengths over multiple brain regions (|genetic correlations| range = (0.21, 0.30), $P < 7.4 \times 10^{-4}$; Fig. 5e and Supplementary Note).

Gene-level association analysis and biological annotations. Gene-level association was tested via MAGMA[80], which detected 714 significant gene–trait associations ($P < 1.5 \times 10^{-9}$, adjusted for 1,777 phenotypes) for 76 genes (Supplementary Fig. 22 and Supplementary Table 11). In addition, we applied FUMA[36] to map significant variants ($P < 2.8 \times 10^{-11}$) to genes via physical position, expression quantitative trait loci association and 3D chromatin Hi-C (high-throughput chromosome conformation capture) interaction, which yielded 193 more associated genes that were not discovered in MAGMA (255 in total; Supplementary Tables 12–15 and Supplementary Note). Four of these intrinsic brain activity-associated genes (*CALY, SLC47A1*, *CYP2C8* and *CYP2C9*) were targets for 11 nervous system drugs[81], such as four psycholeptics (ATC code N05) to produce calming effects, two antidepressants (N06A) to treat MDD and related conditions, two anti-migraine drugs (N02C) and one antidementia drugs (N06D) (Supplementary Table 16).

To identify the tissues and cell types in which genetic variation yields differences in brain functional connectivity, we performed partitioned heritability analyses[82] for tissue type- and cell type-specific regulatory elements[83]. We focused on the ten functional connectivity traits that had heritability higher than 30%. At the FDR 5% level, the most significant enrichments of heritability were observed in active gene regulation regions of fetal brain tissues, neurospheres and neuron/neuronal progenitor cultured cells (Supplementary Fig. 23 and Supplementary Table 17). Among the associated variants of intrinsic brain activity, a few resided in frequently interacting regions and topologically associating domain boundaries in brain tissues[84,85] (Supplementary Table 18). We also performed brain cell type-specific partitioned heritability and gene mapping analyses, the details of which can be found in the Supplementary Note (Supplementary Figs. 24 and 25 and Supplementary Tables 19–21). Finally, MAGMA[80] gene set analysis was performed to prioritize the enriched biological pathways. We found 47 significantly enriched gene sets at the FDR 5% level ($P < 3.2 \times 10^{-6}$; Supplementary Table 22). Multiple pathways related to nervous system were detected, including 'go regulation of glial cell proliferation' (Gene Ontology (GO): 0014009), 'go central nervous system neuron differentiation' (GO: 0021953) and 'go pyramidal neuron differentiation' (GO: 0021859).

Discussion

In the present study, we identified and validated common variants associated with intrinsic brain functions using rsfMRI data of 47,276 subjects, which substantially improves our understanding of the genetic architecture of functional human brain. We used two ICA parcellations with different dimensionalities (25 and 100, respectively)[18,21]. The 25-dimension ICA aimed to build a large-scale network decomposition to match canonical RSNs, and the 100-dimension ICA resulted in a more finely detailed parcellation[6,33]. We then selected 76 (21 + 55) ICA regions that were manually examined to be biologically meaningful[4], which have been widely applied in neuroimaging studies[30]. The ICA regions of the two parcellations were closely related, but they may not have one-to-one correspondence. For example, we found that five ICA region pairs from the two parcellations had very similar spatial locations (correlations of ICA loadings > 0.8), and all of them showed high concordance in downstream GWAS analyses. For other ICA regions, typically, they were linear combinations of a few regions in the other parcellation (Supplementary Table 23 and Supplementary Fig. 26).

Our study faces a few limitations. First, the samples in our discovery GWASs were mainly from individuals with European ancestry. In our PRS analysis, we illustrated a relatively poor replication of the European-ancestry GWAS results within validation cohorts with non-European ancestry. The non-European-ancestry GWAS was of small sample size, so population-specific influences will be better understood when more data from global populations become available[86]. In addition, artificial factors and confounding variables may also weaken the consistency of our results and cause additional challenges in multisite imaging studies[87,88]. Second, we applied group ICA in this study, which was a popular approach to characterize the functionally connected brain[3]. Although the ICA is powerful, it is a data-driven method, which might limit the interpretability of ICA regions and the ability to compare with the patterns observed from parcellation-based studies. For example, the high heritability of the triple networks reported in this paper may partially result from the fact that the ICA captures and combines large variations from different brain networks, because most of the ICA regions distributed across multiple regions and networks. In contrast, parcellation-based analysis typically estimates the heritability independently for each network, which may result in different heritability patterns across the brain[89]. Future studies may explore other parcellation schemes (e.g., the Schaefer parcellation[90]) in the UKB study and examine the robustness of GWAS results to the selection of atlas. Finally, although we found genetic links between brain function and brain structure using tract-based diffusion neuroimaging traits from the existing ENIGMA-DTI pipeline[91,92], a better approach might be developing new pipelines to directly construct structural connectivity matrix for the 76 ICA regions. We expect that accumulating publicly available imaging genetics data resources and more powerful feature extraction pipelines will lead to a better understanding of specific genes involved in human brain structure–function relationships and how variants can alter these relationships, leading to risk of neuropsychiatric disorders.

Online content

Any methods, additional references, Nature Research reporting summaries, source data, extended data, supplementary information, acknowledgements, peer review information; details of author contributions and competing interests; and statements of data and code availability are available at https://doi.org/10.1038/s41588-022-01039-6.

Received: 21 December 2020; Accepted: 28 February 2022;
Published online: 7 April 2022

References

1. Petersen, S. E. & Sporns, O. Brain networks and cognitive architectures. *Neuron* **88**, 207–219 (2015).
2. van den Heuvel, M. P. & Sporns, O. Network hubs in the human brain. *Trends Cogn. Sci.* **17**, 683–696 (2013).
3. Lv, H. et al. Resting-state functional MRI: everything that nonexperts have always wanted to know. *Am. J. Neuroradiol.* **39**, 1390–1399 (2018).
4. Alfaro-Almagro, F. et al. Image processing and quality control for the first 10,000 brain imaging datasets from UK Biobank. *NeuroImage* **166**, 400–424 (2018).
5. Finn, E. S. et al. Functional connectome fingerprinting: identifying individuals using patterns of brain connectivity. *Nat. Neurosci.* **18**, 1664–1671 (2015).
6. Smith, S. M. et al. Correspondence of the brain's functional architecture during activation and rest. *Proc. Natl Acad. Sci. USA* **106**, 13040–13045 (2009).
7. Yeo, B. T. et al. The organization of the human cerebral cortex estimated by intrinsic functional connectivity. *J. Neurophysiol.* **106**, 1125–1165 (2011).
8. Menon, V. Large-scale brain networks and psychopathology: a unifying triple network model. *Trends Cogn. Sci.* **15**, 483–506 (2011).
9. Menon, V. The triple network model, insight, and large-scale brain organization in autism. *Biol. Psychiatry* **84**, 236–238 (2018).
10. Badhwar, A. et al. Resting-state network dysfunction in Alzheimer's disease: a systematic review and meta-analysis. *Alzheimers Dement. (Amst).* **8**, 73–85 (2017).
11. Wolters, A. F. et al. Resting-state fMRI in Parkinson's disease patients with cognitive impairment: a meta-analysis. *Parkinsonism Relat. Disord.* **62**, 16–27 (2019).
12. Mulders, P. C., van Eijndhoven, P. F., Schene, A. H., Beckmann, C. F. & Tendolkar, I. Resting-state functional connectivity in major depressive disorder: a review. *Neurosci. Biobehav. Rev.* **56**, 330–344 (2015).
13. Foo, H. et al. Genetic influence on ageing-related changes in resting-state brain functional networks in healthy adults: a systematic review. *Neurosci. Biobehav. Rev.* **113**, 98–110 (2020).
14. Glahn, D. et al. Genetic control over the resting brain. *Proc. Natl Acad. Sci. USA* **107**, 1223–1228 (2010).
15. Elliott, M. L. et al. General functional connectivity: shared features of resting-state and task fMRI drive reliable and heritable individual differences in functional brain networks. *NeuroImage* **189**, 516–532 (2019).
16. Ge, T., Holmes, A. J., Buckner, R. L., Smoller, J. W. & Sabuncu, M. R. Heritability analysis with repeat measurements and its application to resting-state functional connectivity. *Proc. Natl Acad. Sci. USA* **114**, 5521–5526 (2017).
17. Adhikari, B. M. et al. Heritability estimates on resting state fMRI data using ENIGMA analysis pipeline. In *Pacific Symposium on Biocomputing 2018: Proceedings of the Pacific Symposium* 307-318 (World Scientific, 2018).
18. Elliott, L. T. et al. Genome-wide association studies of brain imaging phenotypes in UK Biobank. *Nature* **562**, 210–216 (2018).
19. Chiesa, P. A. et al. Revolution of resting-state functional neuroimaging genetics in Alzheimer's disease. *Trends Neurosci.* **40**, 469–480 (2017).
20. Zhang, N. et al. APOE and KIBRA interactions on brain functional connectivity in healthy young adults. *Cereb. Cortex* **27**, 4797–4805 (2017).
21. Smith, S. M. et al. An expanded set of genome-wide association studies of brain imaging phenotypes in UK Biobank. *Nat. Neurosci.* **24**, 737–745 (2021).
22. Grasby, K. L. et al. The genetic architecture of the human cerebral cortex.*Science* **367**, eaay6690 (2020).
23. Zhao, B. et al. Genome-wide association analysis of 19,629 individuals identifies variants influencing regional brain volumes and refines their genetic co-architecture with cognitive and mental health traits. *Nat. Genet.* **51**, 1637–1644 (2019).
24. Smith, S. M. & Nichols, T. E. Statistical challenges in "big data" human neuroimaging. *Neuron* **97**, 263–268 (2018).
25. Botvinik-Nezer, R. et al. Variability in the analysis of a single neuroimaging dataset by many teams. *Nature* **582**, 84–88 (2020).
26. Sudlow, C. et al. UK biobank: an open access resource for identifying the causes of a wide range of complex diseases of middle and old age. *PLoS Med.* **12**, e1001779 (2015).
27. Casey, B. et al. The adolescent brain cognitive development (ABCD) study: imaging acquisition across 21 sites. *Developmental Cogn. Neurosci.* **32**, 43–54 (2018).
28. Satterthwaite, T. D. et al. Neuroimaging of the Philadelphia neurodevelopmental cohort. *Neuroimage* **86**, 544–553 (2014).
29. Somerville, L. H. et al. The lifespan human connectome project in development: a large-scale study of brain connectivity development in 5–21 year olds. *NeuroImage* **183**, 456–468 (2018).
30. Miller, K. L. et al. Multimodal population brain imaging in the UK Biobank prospective epidemiological study. *Nat. Neurosci.* **19**, 1523–1536 (2016).
31. Beckmann, C. F. & Smith, S. M. Probabilistic independent component analysis for functional magnetic resonance imaging. *IEEE Trans. Med. Imaging* **23**, 137–152 (2004).
32. Hyvarinen, A. Fast and robust fixed-point algorithms for independent component analysis. *IEEE Trans. Neural Netw.* **10**, 626–634 (1999).
33. Smith, S. M. et al. Resting-state fMRI in the human connectome project. *Neuroimage* **80**, 144–168 (2013).
34. Yang, J., Lee, S. H., Goddard, M. E. & Visscher, P. M. GCTA: a tool for genome-wide complex trait analysis. *Am. J. Hum. Genet.* **88**, 76–82 (2011).
35. Zhao, B. et al. Common genetic variation influencing human white matter microstructure. *Science* **372**, eabf3736 (2021).
36. Watanabe, K., Taskesen, E., Bochoven, A. & Posthuma, D. Functional mapping and annotation of genetic associations with FUMA. *Nat. Commun.* **8**, 1826 (2017).
37. Jansen, I. E. et al. Genome-wide meta-analysis identifies new loci and functional pathways influencing Alzheimer's disease risk. *Nat. Genet.* **51**, 404–413 (2019).
38. Buniello, A. et al. The NHGRI-EBI GWAS Catalog of published genome-wide association studies, targeted arrays and summary statistics 2019. *Nucleic Acids Res.* **47**, D1005–D1012 (2018).
39. Jun, G. R. et al. Transethnic genome-wide scan identifies novel Alzheimer's disease loci. *Alzheimer's Dement.* **13**, 727–738 (2017).
40. Nazarian, A., Yashin, A. I. & Kulminski, A. M. Genome-wide analysis of genetic predisposition to Alzheimer's disease and related sex disparities. *Alzheimer's Res. Ther.* **11**, 5 (2019).
41. Harold, D. et al. Genome-wide association study identifies variants at CLU and PICALM associated with Alzheimer's disease. *Nat. Genet.* **41**, 1088–1093 (2009).
42. Ferrari, R. et al. A genome-wide screening and SNPs-to-genes approach to identify novel genetic risk factors associated with frontotemporal dementia. *Neurobiol. aging* **36**, 2904.e13–2904.e26 (2015).
43. Beecham, G. W. et al. Genome-wide association meta-analysis of neuropathologic features of Alzheimer's disease and related dementias. *PLoS Genet.* **10**, e1004606 (2014).
44. Davies, G. et al. A genome-wide association study implicates the APOE locus in nonpathological cognitive ageing. *Mol. Psychiatry* **19**, 76–87 (2014).
45. Liu, C. et al. Genome-wide association and mechanistic studies indicate that immune response contributes to Alzheimer's disease development. *Front. Genet.* **9**, 410 (2018).
46. Yan, Q. et al. Genome-wide association study of brain amyloid deposition as measured by Pittsburgh Compound-B (PiB)-PET imaging. *Mol. Psychiatry* **26**, 309–321 (2021).
47. Scelsi, M. A. et al. Genetic study of multimodal imaging Alzheimer's disease progression score implicates novel loci. *Brain* **141**, 2167–2180 (2018).
48. Liang, P. et al. Altered amplitude of low-frequency fluctuations in early and late mild cognitive impairment and Alzheimer's disease. *Curr. Alzheimer Res.* **11**, 389–398 (2014).
49. Mattsson, N. et al. Emerging β-amyloid pathology and accelerated cortical atrophy. *JAMA Neurol.* **71**, 725–734 (2014).
50. Pickrell, J. K. et al. Detection and interpretation of shared genetic influences on 42 human traits. *Nat. Genet.* **48**, 709–717 (2016).
51. Consortium, I. P. D. G. Imputation of sequence variants for identification of genetic risks for Parkinson's disease: a meta-analysis of genome-wide association studies. *Lancet* **377**, 641–649 (2011).
52. Vacic, V. et al. Genome-wide mapping of IBD segments in an Ashkenazi PD cohort identifies associated haplotypes. *Hum. Mol. Genet.* **23**, 4693–4702 (2014).
53. Pardiñas, A. F. et al. Common schizophrenia alleles are enriched in mutation-intolerant genes and in regions under strong background selection. *Nat. Genet.* **50**, 381–389 (2018).
54. Hyde, C. L. et al. Identification of 15 genetic loci associated with risk of major depression in individuals of European descent. *Nat. Genet.* **48**, 1031–1036 (2016).
55. Howard, D. M. et al. Genome-wide meta-analysis of depression identifies 102 independent variants and highlights the importance of the prefrontal brain regions. *Nat. Neurosci.* **22**, 343–352 (2019).
56. Anney, R. J. et al. Meta-analysis of GWAS of over 16,000 individuals with autism spectrum disorder highlights a novel locus at 10q24. 32 and a significant overlap with schizophrenia. *Mol. Autism* **8**, 21 (2017).
57. Nagel, M. et al. Meta-analysis of genome-wide association studies for neuroticism in 449,484 individuals identifies novel genetic loci and pathways. *Nat. Genet.* **50**, 920–927 (2018).
58. Baselmans, B. M. et al. Multivariate genome-wide analyses of the well-being spectrum. *Nat. Genet.* **51**, 445–451 (2019).
59. Lane, J. M. et al. Biological and clinical insights from genetics of insomnia symptoms. *Nat. Genet.* **51**, 387–393 (2019).
60. Hill, W. et al. A combined analysis of genetically correlated traits identifies 187 loci and a role for neurogenesis and myelination in intelligence. *Mol. Psychiatry* **24**, 169–181 (2019).

61. Lee, J. J. et al. Gene discovery and polygenic prediction from a genome-wide association study of educational attainment in 1.1 million individuals. *Nat. Genet.* **50**, 1112–1121 (2018).
62. Supekar, K., Cai, W., Krishnadas, R., Palaniyappan, L. & Menon, V. Dysregulated brain dynamics in a triple-network saliency model of schizophrenia and its relation to psychosis. *Biol. Psychiatry* **85**, 60–69 (2019).
63. Zheng, H. et al. The altered triple networks interaction in depression under resting state based on graph theory. *BioMed. Res. Int.* **2015**, 386326 (2015).
64. Uddin, L. Q. et al. Salience network–based classification and prediction of symptom severity in children with autism. *JAMA psychiatry* **70**, 869–879 (2013).
65. Ripke, S. et al. Biological insights from 108 schizophrenia-associated genetic loci. *Nature* **511**, 421–427 (2014).
66. Davies, G. et al. Genome-wide association study of cognitive functions and educational attainment in UK Biobank (N=112 151). *Mol. Psychiatry* **21**, 758–767 (2016).
67. Kichaev, G. et al. Leveraging polygenic functional enrichment to improve GWAS power. *Am. J. Hum. Genet.* **104**, 65–75 (2019).
68. Liu, M. et al. Association studies of up to 1.2 million individuals yield new insights into the genetic etiology of tobacco and alcohol use. *Nat. Genet.* **51**, 237–244 (2019).
69. Savage, J. E. et al. Genome-wide association meta-analysis in 269,867 individuals identifies new genetic and functional links to intelligence. *Nat. Genet.* **50**, 912–919 (2018).
70. Grove, J. et al. Identification of common genetic risk variants for autism spectrum disorder. *Nat. Genet.* **51**, 431–444 (2019).
71. Bulik-Sullivan, B. et al. An atlas of genetic correlations across human diseases and traits. *Nat. Genet.* **47**, 1236–1241 (2015).
72. Binkofski, F. C., Klann, J. & Caspers, S. On the neuroanatomy and functional role of the inferior parietal lobule and intraparietal sulcus. In *Neurobiology of Language* 35–47 (Elsevier, 2016).
73. Cappelletti, M., Lee, H. L., Freeman, E. D. & Price, C. J. The role of right and left parietal lobes in the conceptual processing of numbers. *J. Cogn. Neurosci.* **22**, 331–346 (2010).
74. Koenigs, M., Barbey, A. K., Postle, B. R. & Grafman, J. Superior parietal cortex is critical for the manipulation of information in working memory. *J. Neurosci.* **29**, 14980–14986 (2009).
75. Bijsterbosch, J. D., Beckmann, C. F., Woolrich, M. W., Smith, S. M. & Harrison, S. J. The relationship between spatial configuration and functional connectivity of brain regions revisited. *Elife* **8**, e44890 (2019).
76. Cross-Disorder Group of the Psychiatric Genomics Consortium. Identification of risk loci with shared effects on five major psychiatric disorders: a genome-wide analysis. *Lancet* **381**, 1371–1379 (2013).
77. Zovetti, N. et al. Default mode network activity in bipolar disorder. *Epidemiol. Psychiatr. Sci.* **29**, e166 (2020).
78. Gur, R. E. & Gur, R. C. Functional magnetic resonance imaging in schizophrenia. *Dialogues Clin. Neurosci.* **12**, 333 (2010).
79. Adams, R. A. et al. Impaired theta phase coupling underlies frontotemporal dysconnectivity in schizophrenia. *Brain* **143**, 1261–1277 (2020).
80. de Leeuw, C. A., Mooij, J. M., Heskes, T. & Posthuma, D. MAGMA: generalized gene-set analysis of GWAS data. *PLoS Comput. Biol.* **11**, e1004219 (2015).
81. Wang, Q. et al. A Bayesian framework that integrates multi-omics data and gene networks predicts risk genes from schizophrenia GWAS data. *Nat. Neurosci.* **22**, 691 (2019).
82. Finucane, H. K. et al. Partitioning heritability by functional annotation using genome-wide association summary statistics. *Nat. Genet.* **47**, 1228–1235 (2015).
83. Kundaje, A. et al. Integrative analysis of 111 reference human epigenomes. *Nature* **518**, 317–330 (2015).
84. Schmitt, A. D. et al. A compendium of chromatin contact maps reveals spatially active regions in the human genome. *Cell Rep.* **17**, 2042–2059 (2016).
85. Giusti-Rodriguez, P. M. & Sullivan, P. F. Using three-dimensional regulatory chromatin interactions from adult and fetal cortex to interpret genetic results for psychiatric disorders and cognitive traits. Preprint in *bioRxiv*, https://doi.org/10.1101/406330 (2019).
86. Huang, H. et al. Improving polygenic prediction in ancestrally diverse populations. Preprint in *medRxiv* https://doi.org/10.1101/2020.12.27.20248738 (2020).
87. Fortin, J.-P. et al. Removing inter-subject technical variability in magnetic resonance imaging studies. *Neuroimage* **132**, 198–212 (2016).
88. Alfaro-Almagro, F. et al. Confound modelling in UK Biobank brain imaging. *NeuroImage* **224**, 117002 (2020).
89. Anderson, K. M. et al. Heritability of individualized cortical network topography. *Proc. Natl Acad. Sci. USA* **118**, e2016271118 (2021).
90. Schaefer, A. et al. Local-global parcellation of the human cerebral cortex from intrinsic functional connectivity MRI. *Cereb. cortex* **28**, 3095–3114 (2018).
91. Jahanshad, N. et al. Multi-site genetic analysis of diffusion images and voxelwise heritability analysis: a pilot project of the ENIGMA–DTI working group. *Neuroimage* **81**, 455–469 (2013).
92. Kochunov, P. et al. Multi-site study of additive genetic effects on fractional anisotropy of cerebral white matter: comparing meta and megaanalytical approaches for data pooling. *Neuroimage* **95**, 136–150 (2014).

Methods

Imaging phenotypes and datasets. The rsfMRI datasets were separately processed following the procedures in UKB imaging pipeline[4]. Details about image acquisition, preprocessing and phenotype generation in each dataset can be found in the Supplementary Note. By mapping the preprocessed rsfMRI images onto the pretrained ICA loadings in the previous study[18], we generated two groups of phenotypes, including 76 node amplitude traits reflecting the spontaneous neuronal activity, 1,695 pairwise functional connectivity traits quantifying coactivity for node pairs and 6 global functional connectivity measures to summarize all pairwise functional connectivity. Specifically, we performed a dimension reduction analysis on the 1,695 pairwise functional connectivity traits using a combined principal-component (PC) analysis and ICA approach. The 6 global measures were the top 6 ICA components, which described the whole brain functional connectivity and represented 6 independent sets (i.e., linear combinations) of the 1,695 pairwise functional connectivity traits. To aid interpretation of GWAS results, we manually labeled the 76 functional brain regions characterized in ICA by using the automated anatomical labeling atlas[93] (Supplementary Table 24) and then mapped them onto major functional networks defined in Yeo et al.[7] and Finn et al.[5] (Supplementary Figs. 27 and 28). The assigned location and functional networks are provided in Supplementary Table 25. Details of our mapping procedures are provided in the Supplementary Note. For each continuous phenotype or covariate variable, values greater than five times the median absolute deviation from the median value were removed. We analyzed the following datasets separately: (1) the UKB discovery GWAS, which used data of individuals of British ancestry[94] in the UKB phases 1 to 3 data ($n=34,691$); (2) four European-ancestry validation GWASs, including individuals of white ancestry in the UKB phase 4 data and individuals of white but non-British ancestry in the UKB phases 1 to 3 data (UKBW, $n=5,056$), ABCDE ($n=3,821$), HCP European ($n=495$) and PNC ($n=510$); (3) two non-European-ancestry UKB validation GWASs, including UKBA ($n=446$) and UKBBL ($n=232$); and (4) two non-European-ancestry non-UKB validation GWASs, including ABCDH ($n=768$) and ABCDA ($n=1,257$). See Supplementary Table 26 for a summary of these datasets and demographic information and Supplementary Fig. 29 for an overview of study design. The assignment of ancestry in UKB was based on self-reported ethnicity (Data-Field 21000), which was verified in Bycroft et al.[94]. The ancestry in ABCD was assigned by combining the self-reported ethnicity and ancestry inference results as in Zhao et al.[35].

GWAS discovery and validation. Details of genotyping and quality controls can be found in the Supplementary Note. SNP heritability was estimated by GCTA[34] using all autosomal SNPs in the UKB British cohort. We adjusted for the effects of age (at imaging), age-squared, sex, age–sex interaction, age-squared–sex interaction, imaging site, head location, head motion, head size, long-term drifts and the top 40 genetic PCs. We removed one of a pair of individuals with estimated relatedness larger than 0.025 (using the '—grm-cutoff 0.025' option in GCTA). Genome-wide association analysis was performed using fastGWA[95] while adjusting the same set of covariates as in GCTA. Related individuals were included in fastGWA, and linear mixed-effect model-based approaches were used to account for the sample relatedness. GWASs were separately performed via PLINK[96] in the eight validation datasets, including UKBW, UKBBL, UKBA, ABCDA, ABCDH, ABCDE, HCP European and PNC, where the effects of age, age-squared, sex, head motion, imaging sites (if applicable), head location (if applicable), head size (if applicable), long-term drifts (if applicable), scanners (if applicable), age–sex interaction, age-squared–sex interaction and the top ten genetic PCs were adjusted for. We removed relatives in these validation GWASs.

To validate results in the UKB British discovery GWASs, meta-analysis was performed using the sample size weighted approach via METAL[97]. We examined whether the locus-level associations detected in the British GWAS could be replicated in (1) the UKBW GWAS, (2) the meta-analyzed four European-ancestry validation GWASs (UKBW, ABCDE, HCP European and PNC), (3) the meta-analyzed four non-European-ancestry validation GWAS (UKBBL, UKBA, ABCDA and ABCDH) and (4) the combination of the above eight validation GWASs. Specifically, for each meta-analyzed GWAS, we checked and reported the P value of the 603 top lead independent (LD $r^2<0.1$) associations identified in the UKB British discovery GWASs. PRSs were constructed on eight validation datasets using the lassosum[98]. The summary statistics from UKB British discovery GWAS were used as weights, and the individuals of white ancestry in the UKB phase 4 data were used as validation samples ($n=2,971$). For UKBW, the performance was evaluated on the individuals of white but non-British ancestry in the UKB phases 1 to 3 data ($n=1,940$, removing the relatives of validation samples). Ambiguous variants (i.e., variants with complementary alleles) were removed from analysis. The best prediction accuracy achieved by a single threshold was reported for each phenotype, which was measured by the additional phenotypic variation that can be explained by the polygenic profile (i.e., the incremental R^2) while adjusting for the effects of age, sex, motion and the top ten genetic PCs.

The shared loci and genetic correlation. The genomic loci associated with intrinsic brain activity traits were defined using FUMA (version 1.3.5e). We inputted UKB British discovery summary statistics. To define the LD boundaries, FUMA identified independent significant variants, which were defined as variants with a P value smaller than the predefined threshold that were independent of other significant variants (LD $r^2<0.6$). FUMA then constructed LD blocks for these independent significant variants by tagging all variants in LD ($r^2\geq0.6$) with at least one independent significant variant and had a minor allele frequency ≥0.0005. These variants included those from the 1000 Genomes reference panel that may not have been included in the GWASs. Moreover, within these significant variants, independent lead variants were identified as those that were independent from each other (LD $r^2<0.1$). If LD blocks of independent significant variants were close (<250 kb based on the closest boundary variants of LD blocks), they were merged into a single genomic locus. Thus, each genomic locus could contain multiple significant variants and lead variants. Independent significant variants and all the variants in LD with them ($r^2\geq0.6$) were searched by FUMA on the NHGRI-EBI GWAS catalog (version 2019-09-24) to look for previously reported associations ($P<9\times10^{-6}$) with any traits. LDSC[71] software (version 1.0.1) was used to estimate and test the pairwise genetic correlation. We used the precalculated LD scores provided by LDSC, which were computed using 1000 Genomes European data. We used HapMap3[99] variants and removed all variants in the major histocompatibility complex region. The summary statistics of intrinsic brain activity traits were from the UKB British discovery GWAS, and the resources of other summary statistics are provided in Supplementary Table 9.

Gene-level analysis and biological annotation. Gene-based association analysis was performed in UKB British participants for 18,796 protein-coding genes using MAGMA[80] (version 1.08). Default MAGMA settings were used with zero window size around each gene. We then carried out FUMA functional annotation and mapping analysis, in which variants were annotated with their biological functionality and then were linked to 35,808 candidate genes by a combination of positional, expression quantitative trait loci and 3D chromatin interaction mappings. Brain-related tissues/cells were selected in all options, and default values were used for all other parameters in FUMA. For the detected genes in MAGMA and FUMA, we performed lookups in the NHGRI-EBI GWAS catalog (version 2020-02-08) to explore their previously reported gene–trait associations. We performed heritability enrichment analysis via partitioned LDSC[82]. Baseline models were adjusted when estimating and testing the enrichment scores for our tissue type and cell type-specific annotations. Methods to analysis chromatin data of glial and neuronal cell subtypes can be found in Hauberg et al.[100]. MAGMA was also used to explore the enriched biological pathways, in which we tested 500 curated gene sets and 9,996 GO terms from the Molecular Signatures Database[101] (version 7.0). Additional gene mapping was performed using 14 Hi-C datasets of brain tissue and cell types from five recent studies, including (1) the promoter capture Hi-C data of hippocampus and dorsolateral prefrontal cortex[102]; (2) the Hi-C data of hippocampus and dorsolateral prefrontal cortex[84]; (3) the Hi-C data from fetal and adult cortices[85], restricting to the high confidence interactions; (4) the promoter capture Hi-C data of primary astrocytes and three types of induced pluripotent stem cell-derived neurons[103] (cortical, hippocampal and motor); and (5) proximity ligation-assisted chromatin immunoprecipitation sequencing data on sorted fetal neuron cells[104], including radial glial cells, intermediate progenitor cells, neurons and interneurons. For interaction intensity cutoffs, we used 2 for the $-\log10(P)$ used in datasets of Jung et al.[102], 0.05 for the q value in Schmitt et al.[84] and Giusti-Rodriguez and Sullivan[85], 5 for the Chicago score in Song et al.[103] and 0.01 for the FDR in Song et al.[104].

Reporting Summary. Further information on research design is available in the Nature Research Reporting Summary linked to this article.

Data availability

Our GWAS summary statistics are publicly available at Zenodo[105] (https://doi.org/10.5281/zenodo.5775047). The individual-level imaging and genetics data used in the present study are available from four publicly accessible data resources: UKB (https://www.ukbiobank.ac.uk/), ABCD (https://abcdstudy.org/), HCP (https://www.humanconnectome.org/) and PNC (https://www.med.upenn.edu/bbl/philadelphianeurodevelopmentalcohort.html). The Molecular Signatures Database dataset can be downloaded from https://www.gsea-msigdb.org/gsea/msigdb/. The Hi-C datasets of brain tissue and cell types can be requested or accessed following the instructions in the original publications. Our results can also be easily browsed through our knowledge portal at https://bigkp.org/.

Code availability

We made use of publicly available software and tools listed in URLs. The codes to generate the rsfMRI features are publicly available on Zenodo (https://doi.org/10.5281/zenodo.5784010). Other codes used in our analyses are available upon reasonable request.

References

93. Rolls, E. T., Huang, C.-C., Lin, C.-P., Feng, J. & Joliot, M. Automated anatomical labelling atlas 3. *NeuroImage* **206**, 116189 (2020).
94. Bycroft, C. et al. The UK Biobank resource with deep phenotyping and genomic data. *Nature* **562**, 203–209 (2018).

95. Jiang, L. et al. A resource-efficient tool for mixed model association analysis of large-scale data. *Nat. Genet.* **51**, 1749–1755 (2019).
96. Purcell, S. et al. PLINK: a tool set for whole-genome association and population-based linkage analyses. *Am. J. Hum. Genet.* **81**, 559–575 (2007).
97. Willer, C. J., Li, Y. & Abecasis, G. R. METAL: fast and efficient meta-analysis of genomewide association scans. *Bioinformatics* **26**, 2190–2191 (2010).
98. Mak, T. S. H., Porsch, R. M., Choi, S. W., Zhou, X. & Sham, P. C. Polygenic scores via penalized regression on summary statistics. *Genet. Epidemiol.* **41**, 469–480 (2017).
99. International HapMap 3 Consortium. Integrating common and rare genetic variation in diverse human populations. *Nature* **467**, 52–58 (2010).
100. Hauberg, M. E. et al. Common schizophrenia risk variants are enriched in open chromatin regions of human glutamatergic neurons. *Nat. Commun.* **11**, 5581 (2020).
101. Liberzon, A. et al. Molecular Signatures Database (MSigDB) 3.0. *Bioinformatics* **27**, 1739–1740 (2011).
102. Jung, I. et al. A compendium of promoter-centered long-range chromatin interactions in the human genome. *Nat. Genet.* **51**, 1442–1449 (2019).
103. Song, M. et al. Mapping cis-regulatory chromatin contacts in neural cells links neuropsychiatric disorder risk variants to target genes. *Nat. Genet.* **51**, 1252–1262 (2019).
104. Song, M. et al. Cell-type-specific 3D epigenomes in the developing human cortex. *Nature* **587**, 644–649 (2020).
105. Zhao, B. et al. GWAS summary statistics for 191 resting-state functional MRI (rs-fMRI) traits. *Zenodo* https://doi.org/10.5281/zenodo.5775047 (2021).

Acknowledgements

This research was partially supported by National Institutes of Health (NIH) grants MH086633 (H.Z.) and MH116527 (T. Li). We thank the individuals represented in the UKB, ABCD, HCP and PNC studies for their participation and the research teams for their work in collecting, processing and disseminating these datasets for analysis. We gratefully acknowledge all the studies and databases that made GWAS summary data available. This research has been conducted using the UKB resource (application number 22783), subject to a data transfer agreement. Some data used in the preparation of this article were obtained from the ABCD study (https://abcdstudy.org), held in the National Institute of Mental Health Data Archive. This is a multisite, longitudinal study designed to recruit more than 10,000 children age 9–10 years and follow them over 10 years into early adulthood. The ABCD study is supported by the NIH and additional federal partners under award numbers U01DA041022, U01DA041028, U01DA041048, U01DA041089, U01DA041106, U01DA041117, U01DA041120, U01DA041134, U01DA041148, U01DA041156, U01DA041174, U24DA041123, U24DA041147, U01DA041093 and U01DA041025. A full list of supporters is available at https://abcdstudy.org/federal-partners.html. A listing of participating sites and a complete listing of the study investigators can be found at https://abcdstudy.org/scientists/workgroups/. ABCD consortium investigators designed and implemented the study and/or provided data but did not necessarily participate in analysis or writing of this report. This article reflects the views of the authors and may not reflect the opinions or views of the NIH or ABCD consortium investigators. Support for the collection of the PNC datasets was provided by grant RC2MH089983 awarded to Raquel Gur and RC2MH089924 awarded to H. Hakonarson. All PNC subjects were recruited through the Center for Applied Genomics at The Children's Hospital in Philadelphia. HCP data were provided by the HCP, WU-Minn Consortium (principal investigators D. Van Essen and K. Ugurbil; 1U54MH091657) funded by the 16 NIH institutes and centers that support the NIH Blueprint for Neuroscience Research and the McDonnell Center for Systems Neuroscience at Washington University. The UKB study has obtained ethics approval from the North West Multi-Centre Research Ethics Committee (approval number 11/NW/0382) and obtained written informed consent from all participants before the study. All experimental procedures in the HCP study were approved by the institutional review boards at Washington University (approval number 201204036). All procedures in the ABCD study were approved by the institutional review boards at ABCD collection sites (approval numbers 201708123 and 160091). The institutional review boards of the University of Pennsylvania and the Children's Hospital of Philadelphia approved all study procedures in the PNC study.

Author contributions

B.Z., H.Z., J.L.S., S.M.S., and Y.L. designed the study. B.Z., T. Li, D.X., X.W., Yue Yang, T. Luo, N.M., Q.S. and Yuchen Yang analyzed the data. T. Li, Z.Z. and Y.S. downloaded the datasets, processed rsfMRI data and undertook quantity controls. W.L. assisted in interpreting findings. P.R., M.E.H., J.B. and J.F.F. analyzed brain cell chromatin accessibility data. B.Z. wrote the manuscript, with feedback from all authors.

Competing interests

The authors declare no competing interests.

Additional information

Extended data is available for this paper at https://doi.org/10.1038/s41588-022-01039-6.

Supplementary information The online version contains supplementary material available at https://doi.org/10.1038/s41588-022-01039-6.

Correspondence and requests for materials should be addressed to Hongtu Zhu.

Peer review information *Nature Genetics* thanks the anonymous reviewers for their contribution to the peer review of this work. Peer reviewer reports are available.

Reprints and permissions information is available at www.nature.com/reprints.

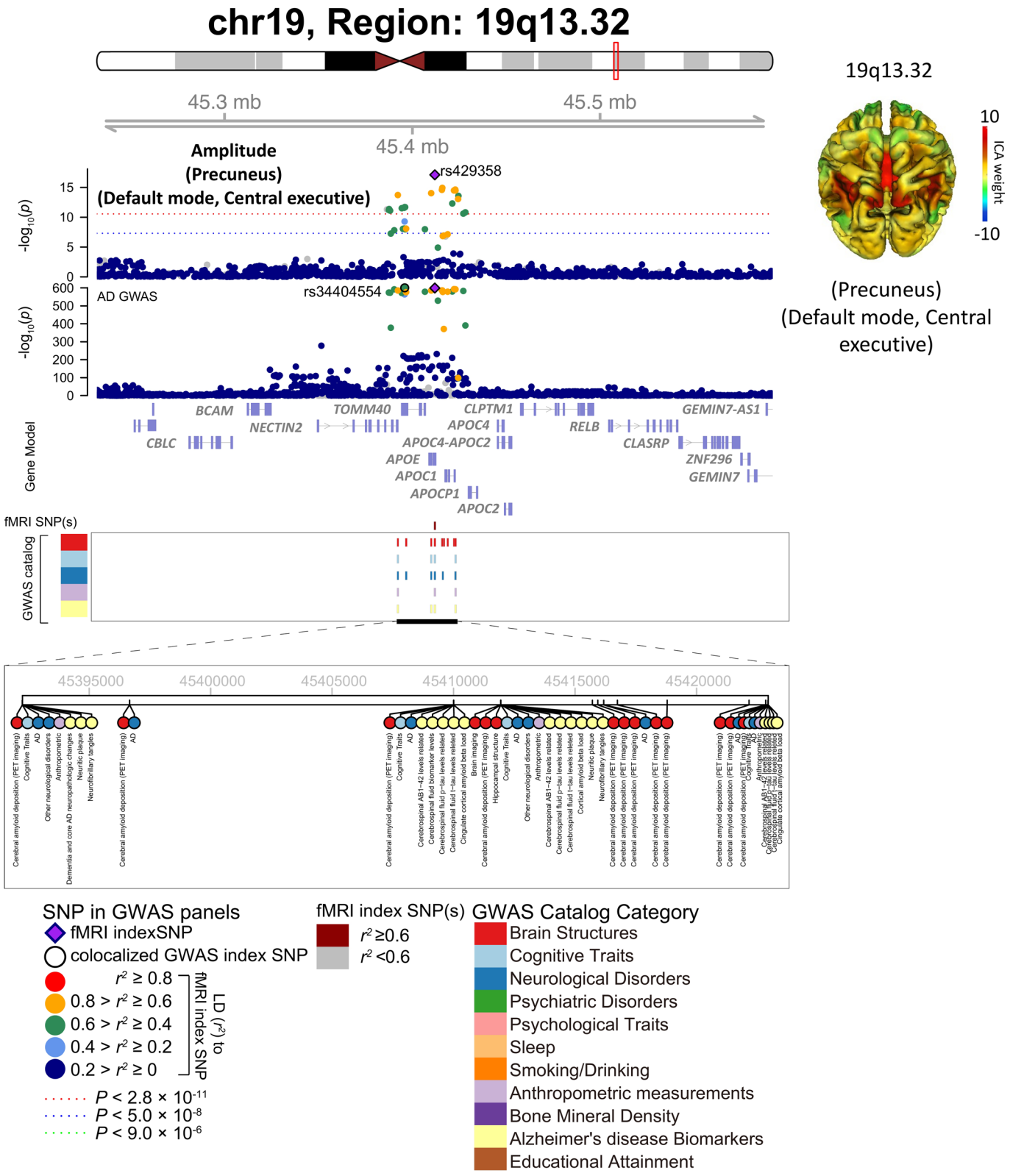

Extended Data Fig. 1 | Genetic locus at 19q13.21 associated with both rsfMRI trait of brain activity and brain-related complex traits and disorders. At 19q13.32, we observed colocalization (LD $r^2 \geq 0.6$) between the amplitude of the precuneus region in the default mode and central executive networks and Alzheimer's disease (shared index SNP rs429358). Location of the displayed rsfMRI trait (amplitude of the precuneus) is illustrated in the right panel.

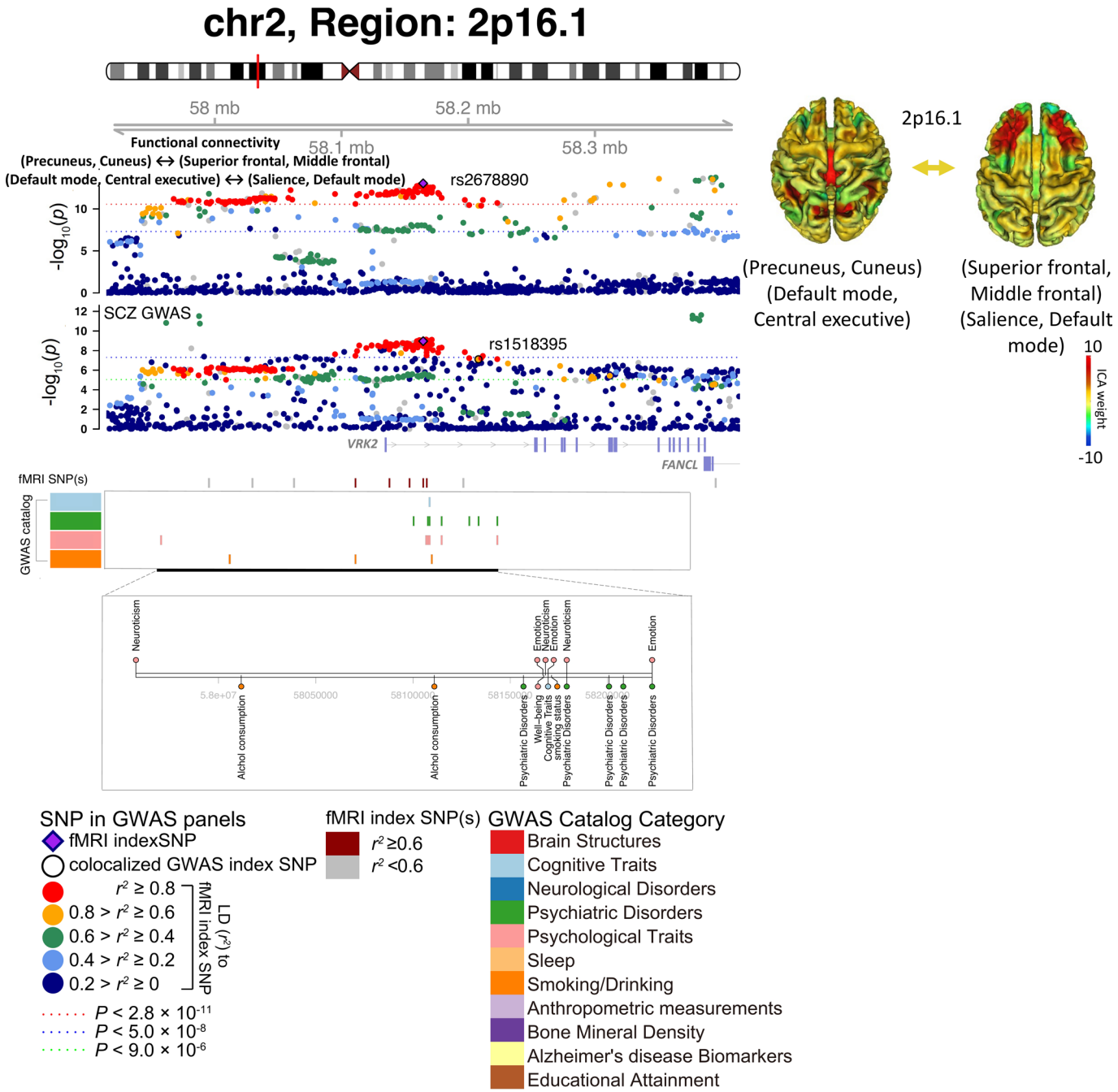

Extended Data Fig. 2 | Genetic locus at 2p16.1 associated with both rsfMRI trait of brain activity and brain-related complex traits and disorders. At 2p16.1, we observed colocalization (LD $r^2 \geq 0.6$) between the functional connectivity among the default mode, central executive, and salience networks (index SNP rs2678890) and schizophrenia (index SNP rs1518395). Location of the displayed rsfMRI trait (functional connectivity between precuneus & cuneus and superior frontal & middle frontal regions) is illustrated in the right panel.

nature research

Corresponding author(s): Hongtu Zhu

Last updated by author(s): December 13, 2021

Reporting Summary

Nature Research wishes to improve the reproducibility of the work that we publish. This form provides structure for consistency and transparency in reporting. For further information on Nature Research policies, see our Editorial Policies and the Editorial Policy Checklist.

Statistics

For all statistical analyses, confirm that the following items are present in the figure legend, table legend, main text, or Methods section.

n/a	Confirmed
☐	☒ The exact sample size (*n*) for each experimental group/condition, given as a discrete number and unit of measurement
☐	☒ A statement on whether measurements were taken from distinct samples or whether the same sample was measured repeatedly
☐	☒ The statistical test(s) used AND whether they are one- or two-sided *Only common tests should be described solely by name; describe more complex techniques in the Methods section.*
☐	☒ A description of all covariates tested
☐	☒ A description of any assumptions or corrections, such as tests of normality and adjustment for multiple comparisons
☐	☒ A full description of the statistical parameters including central tendency (e.g. means) or other basic estimates (e.g. regression coefficient) AND variation (e.g. standard deviation) or associated estimates of uncertainty (e.g. confidence intervals)
☐	☒ For null hypothesis testing, the test statistic (e.g. *F*, *t*, *r*) with confidence intervals, effect sizes, degrees of freedom and *P* value noted *Give P values as exact values whenever suitable.*
☐	☒ For Bayesian analysis, information on the choice of priors and Markov chain Monte Carlo settings
☐	☒ For hierarchical and complex designs, identification of the appropriate level for tests and full reporting of outcomes
☐	☒ Estimates of effect sizes (e.g. Cohen's *d*, Pearson's *r*), indicating how they were calculated

Our web collection on statistics for biologists contains articles on many of the points above.

Software and code

Policy information about availability of computer code

Data collection	UKB Imaging Pipeline (version 1), https://git.fmrib.ox.ac.uk/falmagro/UK_biobank_pipeline_v_1; UK Biobank Brain Imaging - Online Resources, https://www.fmrib.ox.ac.uk/ukbiobank;
Data analysis	Codes to generate rsfMRI features, https://doi.org/10.5281/zenodo.5775047; METAL (version March 2011), https://genome.sph.umich.edu/wiki/METAL ; PLINK (version 2), https://www.cog-genomics.org/plink2/; GCTA (1.91.7beta) & fastGWA (1.93.0beta), http://cnsgenomics.com/software/gcta/; FUMA (version 1.3.5e), http://fuma.ctglab.nl/; MAGMA (version 1.08), https://ctg.cncr.nl/software/magma; LDSC (version 1.0.1), https://github.com/bulik/ldsc/; NHGRI-EBI (version 2020-02-08), GWAS Catalog, https://www.ebi.ac.uk/gwas/home;

For manuscripts utilizing custom algorithms or software that are central to the research but not yet described in published literature, software must be made available to editors and reviewers. We strongly encourage code deposition in a community repository (e.g. GitHub). See the Nature Research guidelines for submitting code & software for further information.

Data

Policy information about availability of data

All manuscripts must include a data availability statement. This statement should provide the following information, where applicable:

- Accession codes, unique identifiers, or web links for publicly available datasets
- A list of figures that have associated raw data
- A description of any restrictions on data availability

Our GWAS summary statistics are publicly available at Zenodo (https://doi.org/10.5281/zenodo.5775047). The individual-level imaging and genetics data used in the present study are available from four publicly accessible data resources: UK Biobank (https://www.ukbiobank.ac.uk/), ABCD (https://abcdstudy.org/), PNC (https://www.med.upenn.edu/bbl/philadelphianeurodevelopmentalcohort.html), and HCP (https://www.humanconnectome.org/). The MSigDB dataset can be downloaded from https://www.gsea-msigdb.org/gsea/msigdb/. The Hi-C datasets of brain tissue and cell types can be requested or accessed following the instructions in the original publications. Our results can also be easily browsed through our knowledge portal https://bigkp.org/.

Field-specific reporting

Please select the one below that is the best fit for your research. If you are not sure, read the appropriate sections before making your selection.

☒ Life sciences ☐ Behavioural & social sciences ☐ Ecological, evolutionary & environmental sciences

For a reference copy of the document with all sections, see nature.com/documents/nr-reporting-summary-flat.pdf

Life sciences study design

All studies must disclose on these points even when the disclosure is negative.

Sample size	No power calculation was needed in advance. We used all data passing standard quality controls (please see below), which resulted in 47,276 individuals. The sample size in our study was greater than that of most of the previous GWAS on brain rsfMRI traits.
Data exclusions	Full details of data exclusions can be found in the Methods section and Supplementary Note. For the genetic SNP data, we performed the following SNP data quality controls on each dataset: 1) exclude subjects with more than 10% missing genotypes; 2) exclude SNPs with minor allele frequency less than 0.01; 3) exclude SNPs with larger than 10% missing genotyping rate; 4) exclude markers that failure the Hardy-Weinberg test and 5) remove SNPs with imputation INFO score less than 0.8. For imaging data, we performed standard imaging quality controls in UKB Imaging Pipeline. For each continuous phenotype or covariate variable, we removed values greater than five times the median absolute deviation from the median value.
Replication	For discovery, we used the GWAS sresults of the UKB British cohort (n = 34,691). Then the data from other studies were used for validation in various analyses (n=12,585). Specifically, we checked whether the 603 significant locus-trait associations detected in UKB British cohort can be replicated. We found that 118 associations (19.6%) passed the Bonferroni significance level in the European validation dataset, and 440 (73.0%) were significant at the nominal 0.05 level. All the 440 associations had concordant directions in the two independent GWAS, showing a high degree of generalizability of our GWAS findings among European cohorts. We also performed replication in non-European validation dataset and found that one association passed the Bonferroni significance level and 34 (5.6%) were significant at the nominal 0.05 level and had the same direction as in UKB British cohort. The lower degree of generalizability in non-European analysis may be related to the small sample size of non-European datasets and the potential population specific influences on brain function in non-European cohorts.
Randomization	All the datasets are from observational studies, and we used all samples available after data exclusions listed above. Therefore, there is no equivalent process of randomization in the present analysis.
Blinding	The data are not from controlled randomized studies, thus there is no step equivalent to blinding involved.

Reporting for specific materials, systems and methods

We require information from authors about some types of materials, experimental systems and methods used in many studies. Here, indicate whether each material, system or method listed is relevant to your study. If you are not sure if a list item applies to your research, read the appropriate section before selecting a response.

Materials & experimental systems

n/a	Involved in the study
☒	☐ Antibodies
☒	☐ Eukaryotic cell lines
☒	☐ Palaeontology and archaeology
☒	☐ Animals and other organisms
☐	☒ Human research participants
☒	☐ Clinical data
☒	☐ Dual use research of concern

Methods

n/a	Involved in the study
☒	☐ ChIP-seq
☒	☐ Flow cytometry
☐	☒ MRI-based neuroimaging

Human research participants

Policy information about studies involving human research participants

Population characteristics	The main GWAS made use of data of individuals of British ancestry from the UKB study, the UKB genetic data have ~9m SNPs after genotyping quality controls, all individuals were ages between 40 and 80 with mean 62.51, the proportion of male is 0.47. See Supplementary Table 26 for a summary of sample size and demographic information of each cohort.
Recruitment	Recruitment details and dataset overviews can be found in https://doi.org/10.1371/journal.pmed.1001779 for UKB, https://doi.org/10.1016/j.neuroimage.2013.07.064 for PNC, https://doi.org/10.1016/j.neuroimage.2018.08.050 for HCP, and https://doi.org/10.1016/j.dcn.2018.03.001 for ABCD.
Ethics oversight	The UKB study has obtained ethics approval from the North West Multi-Centre Research Ethics Committee (MREC, approval number: 11/NW/0382), and obtained written informed consent from all participants prior to the study. All experimental procedures in the HCP study were approved by the institutional review boards at Washington University (approval number: 201204036). All procedures in the ABCD study were approved by the institutional review boards at ABCD collection sites (approval numbers: 201708123 and 160091). The institutional review boards of the University of Pennsylvania and the Children's Hospital of Philadelphia approved all study procedures in the PNC study.

Note that full information on the approval of the study protocol must also be provided in the manuscript.

Magnetic resonance imaging

Experimental design

Design type	This study made use of imaging data from resting-state functional MRI and genetic SNP data.
Design specifications	Details can be found in Miller et al. (doi:10.1038/nn.4393) and Alfaro-Almagro et al. (https://doi.org/10.1016/j.neuroimage.2017.10.034) for UKB, https://doi.org/10.1016/j.neuroimage.2013.07.064 for PNC, https://doi.org/10.1016/j.neuroimage.2018.08.050 for HCP, and https://doi.org/10.1016/j.dcn.2018.03.001 for ABCD.
Behavioral performance measures	Behavioral performance measures were not used in this study.

Acquisition

Imaging type(s)	resting-state functional MRI
Field strength	3T in UKB, PNC, and HCP; at least 3T for ABCD.
Sequence & imaging parameters	Details can be found in Miller et al. (doi:10.1038/nn.4393) and Alfaro-Almagro et al. (https://doi.org/10.1016/j.neuroimage.2017.10.034) for UKB, https://doi.org/10.1016/j.neuroimage.2013.07.064 for PNC, https://doi.org/10.1016/j.neuroimage.2018.08.050 for HCP, and https://doi.org/10.1016/j.dcn.2018.03.001 for ABCD.
Area of acquisition	The whole brain scan was used.

Diffusion MRI ☐ Used ☒ Not used

Preprocessing

Preprocessing software	Details can be found in Miller et al. (doi:10.1038/nn.4393) and Alfaro-Almagro et al. (https://doi.org/10.1016/j.neuroimage.2017.10.034) for UKB, https://doi.org/10.1016/j.neuroimage.2013.07.064 for PNC, https://doi.org/10.1016/j.neuroimage.2018.08.050 for HCP, and https://doi.org/10.1016/j.dcn.2018.03.001 for ABCD.
Normalization	Details can be found in Miller et al. (doi:10.1038/nn.4393) and Alfaro-Almagro et al. (https://doi.org/10.1016/j.neuroimage.2017.10.034) for UKB, https://doi.org/10.1016/j.neuroimage.2013.07.064 for PNC, https://doi.org/10.1016/j.neuroimage.2018.08.050 for HCP, and https://doi.org/10.1016/j.dcn.2018.03.001 for ABCD.
Normalization template	Details can be found in Miller et al. (doi:10.1038/nn.4393) and Alfaro-Almagro et al. (https://doi.org/10.1016/

Normalization template	j.neuroimage.2017.10.034) for UKB, https://doi.org/10.1016/j.neuroimage.2013.07.064 for PNC, https://doi.org/10.1016/j.neuroimage.2018.08.050 for HCP, and https://doi.org/10.1016/j.dcn.2018.03.001 for ABCD.
Noise and artifact removal	Details can be found in Miller et al. (doi:10.1038/nn.4393) and Alfaro-Almagro et al. (https://doi.org/10.1016/j.neuroimage.2017.10.034) for UKB, https://doi.org/10.1016/j.neuroimage.2013.07.064 for PNC, https://doi.org/10.1016/j.neuroimage.2018.08.050 for HCP, and https://doi.org/10.1016/j.dcn.2018.03.001 for ABCD.
Volume censoring	Details can be found in Miller et al. (doi:10.1038/nn.4393) and Alfaro-Almagro et al. (https://doi.org/10.1016/j.neuroimage.2017.10.034) for UKB, https://doi.org/10.1016/j.neuroimage.2013.07.064 for PNC, https://doi.org/10.1016/j.neuroimage.2018.08.050 for HCP, and https://doi.org/10.1016/j.dcn.2018.03.001 for ABCD.

Statistical modeling & inference

Model type and settings	Details can be found in Miller et al. (doi:10.1038/nn.4393) and Alfaro-Almagro et al. (https://doi.org/10.1016/j.neuroimage.2017.10.034) for UKB, https://doi.org/10.1016/j.neuroimage.2013.07.064 for PNC, https://doi.org/10.1016/j.neuroimage.2018.08.050 for HCP, and https://doi.org/10.1016/j.dcn.2018.03.001 for ABCD.
Effect(s) tested	Details can be found in Miller et al. (doi:10.1038/nn.4393) and Alfaro-Almagro et al. (https://doi.org/10.1016/j.neuroimage.2017.10.034) for UKB, https://doi.org/10.1016/j.neuroimage.2013.07.064 for PNC, https://doi.org/10.1016/j.neuroimage.2018.08.050 for HCP, and https://doi.org/10.1016/j.dcn.2018.03.001 for ABCD.

Specify type of analysis: ☐ Whole brain ☐ ROI-based ☒ Both

Anatomical location(s): See https://www.fmrib.ox.ac.uk/ukbiobank/ and https://doi.org/10.1016/j.neuroimage.2019.116189

Statistic type for inference (See Eklund et al. 2016)	Inference was not carried out when generating imaging phenotypes.
Correction	Inference was not carried out when generating imaging phenotypes.

Models & analysis

n/a	Involved in the study
☐	☒ Functional and/or effective connectivity
☒	☐ Graph analysis
☒	☐ Multivariate modeling or predictive analysis

Functional and/or effective connectivity: functional connectivity